CO2 ARC BEHAVIOR DURING CURRENT INTERRUPTION PROCESS IN A GAS CIRCUIT BREAKER WITH EXTERNALLY APPLIED MAGNETIC FIELD

T. TAKEMATSU[1]*, S. HIRAYAMA[1], T. FUJINO[1], M. ISHIKAWA[1]
S. OGAWA[2], AND T. MORI[2]

[1] *University of Tsukuba, Tsukuba, 305-8573, Japan,* takematsu@fmm.kz.tsukuba.ac.jp
[2] *Toshiba Corporation, Kawasaki, 210-0862, Japan*

ABSTRACT

The authors conduct three-dimensional and time dependent magnetohydrodynamic numerical simulations of a gas circuit breaker model with externally applied magnetic field for CO_2 or SF_6 gas. The objective of this work is to examine the current interruption process of the gas circuit breaker model with the applied magnetic field for both gases. Numerical results show that applying the magnetic field induces swirl flow, which leads to the pressure rise in the puffer chamber for both gases. Just before second current zero, the arc forms cylindrical shape under the magnetic field for CO_2 gas unlike SF_6 gas where the arc column forms spiral shape. Arc conductance around the time is reduced by applying the magnetic field for both gases because heat convection around the arc is enhanced. This means that the thermal interruption capability can be improved by applying the magnetic field for both gases.

1. INTRODUCTION

SF_6 gas has been used as the arc interruption medium in most high-voltage gas circuit breakers (GCB). CO_2 gas is, however, considered as a possible SF_6 alternatives because the global warming potential of CO_2 gas is much smaller than that of SF_6 gas. Recently, eco-friendly gas circuit breakers using CO_2 gas have been developed (e.g., [1, 2]). Uchii et al. developed a CO_2-GCB model, and it achieved practical levels of performance for major test-duties [1]. Methods including optimization of GCB design which can use arc energy for puffer pressure rise are needed for a CO_2-GCB because the intrinsic current interruption capability of CO_2 gas is inferior to that of SF_6 gas.
The authors propose the utilization of externally applied magnetic field in a CO_2-GCB to improve current interruption capability. Under magnetic field, arc is driven by Lorentz force in a gas. As a result, convective heat transfer from the arc to a surrounding gas is expected to be promoted. This effect leads to a rise in pressure in a puffer chamber and a decrease in arc conductance.

The objective of this work is to examine arc behavior and decaying process of arc conductance under magnetic field in current interruption process for a GCB model using CO_2 gas or SF_6 gas.

2. NUMERICAL PROCEDURE

The governing equations for conservative variables are written as follows.

Mass conservation equation:

$$\frac{\partial}{\partial t}\int_V \rho dV + \oint_S \rho(\boldsymbol{u}-\boldsymbol{g})\cdot\boldsymbol{n}dS = 0 \tag{1}$$

Momentum conservation equation:

$$\frac{\partial}{\partial t}\int_V \rho\boldsymbol{u}dV + \oint_S \rho\boldsymbol{u}(\boldsymbol{u}-\boldsymbol{g})\cdot\boldsymbol{n}dS = \int_V (\boldsymbol{J}\times\boldsymbol{B})dV - \oint_S p\boldsymbol{n}dS + \oint_S \tau\cdot\boldsymbol{n}dS = 0 \tag{2}$$

Energy conservation equations:

$$\frac{\partial}{\partial t}\int_V \rho\hat{E}dV + \oint_S \rho\hat{H}(\boldsymbol{u}-\boldsymbol{g})\cdot\boldsymbol{n}dS = \oint_S \kappa(\nabla T\cdot\boldsymbol{n})dS + \int_V (\boldsymbol{J}\cdot\boldsymbol{E} - \dot{q}_{rad})dV - \oint_S p(\boldsymbol{g}\cdot\boldsymbol{n})dS + \oint_S (\tau\cdot\boldsymbol{u})\cdot\boldsymbol{n}dS \tag{3}$$

where p is the pressure, T the temperature. τ is the viscous stress tensor. $\boldsymbol{u}$, $\boldsymbol{J}$, $\boldsymbol{E}$, and

$\boldsymbol{B}$ are the vector of the velocity, the electric current density, the electric field strength, and the magnetic flux density, respectively. ρ is the mass density, $\hat{E}$ the total internal energy per unit mass, $\hat{H}$ the total enthalpy per unit mass, κ the thermal conductivity, and $\dot{q}_{rad}$ the radiation heat loss, respectively. V is the cell volume, S the cell surface area, $\boldsymbol{g}$ the velocity vector of cell boundary, $\boldsymbol{n}$ the normal unit vector. The thermodynamic properties, the transport coefficients, and the emission coefficient of SF_6 and CO_2 gases are formulated as a function of temperature and pressure. The numerical simulation can deal with the movement of the arcing contact and complex shapes such as puffer chamber by using Cut-Cell method [3, 4]. Eqs. (1)—(3) are solved with the finite volume method. For electrodynamics, the governing equations are written as follows.

$$\boldsymbol{E} = -\nabla\phi \tag{4}$$

$$\nabla \cdot \boldsymbol{J} = 0 \tag{5}$$

$$\boldsymbol{J} = \sigma(\boldsymbol{E} + \boldsymbol{u} \times \boldsymbol{B}) \tag{6}$$

where ϕ is the scalar potential [V], σ the electric conductivity [S/m]. The potential differential equation derived from Eqs. (4)-(6) is discretized by the Galerkin finite element method.

The analysis object as shown in Fig. 1 is based on the SF_6 rotary arc type interruption chamber used by Mori et al [5]. Time variation of arc current and the externally applied magnetic flux density assigned in this work are shown in Fig. 2, and Fig. 3, respectively. The maximum magnetic flux density on the surface of the arc-runner is about 0.14 T. Top of the movable arcing contact moves from x = 0.071 m (t = 0 ms) to x = 0.133 m (t = 20.05 ms).

On the wall surface, the non-slip wall condition is assumed. The wall temperature is set to 300 K. The electrical potential is set to 0 V on the surface of the movable arcing contact, and it is also determined to apply the setting arc current on the surface of stationary contact and arc-runner. The pressure and the temperature are set to 0.5 MPa and 300 K, respectively, for the boundary condition in the opening area ($x \geq 0.12\,\mathrm{m}$). In the space filled with the working gas, the pressure and the temperature are set to 0.5 MPa and 300 K, respectively, for the initial condition. A heat energy is artificially added between the electrode gap to make a discharge path during t = 0-0.20 ms. After that, the arc current as shown in Fig. 2 is applied.

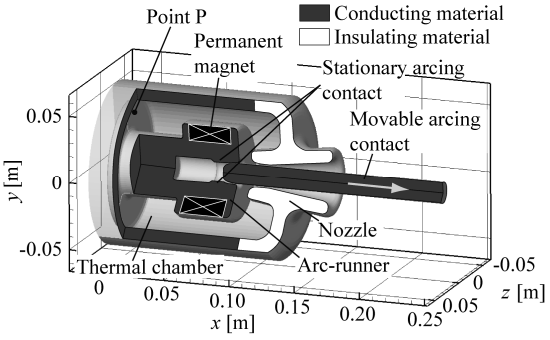

Fig. 1 Configuration of the model arc extinguishing chamber

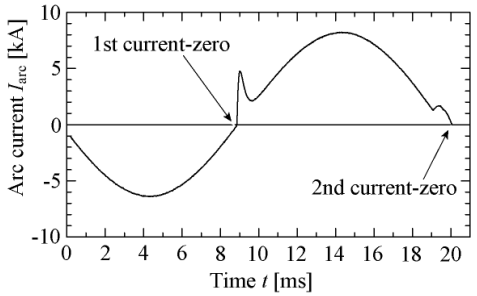

Fig. 2 Time variation of arc current

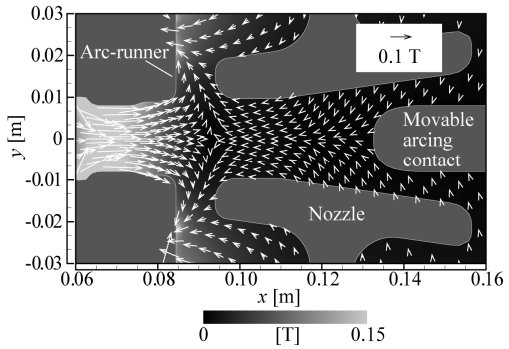

Fig. 3 Two-dimensional distribution of externally applied magnetic flux density on x-y plane (z = 0 m)

3. NUMERICAL RESULTS AND DISCUSSION

Figure 4 shows three-dimensional views of the isosurfaces of T = 5000 and 10000 K at t = 15.0 ms (around the current maximum point) and 20.0 ms (just before second current-zero point). We approximately regard the isosurface of T = 5000 K as the edge of arc plasma. In Fig. 4(a) and Fig. 4(b), high temperature region ($T \geq 5000\,\mathrm{K}$) around the nozzle is decreased by applying the magnetic field for CO_2 gas. In addition, the high temperature region is expanded on the surface of arc-runner under the applied magnetic field. These characteristics can be also confirmed in the case of SF_6. Comparing Fig. 4(a) with Fig. 4(c), however, the arc forms

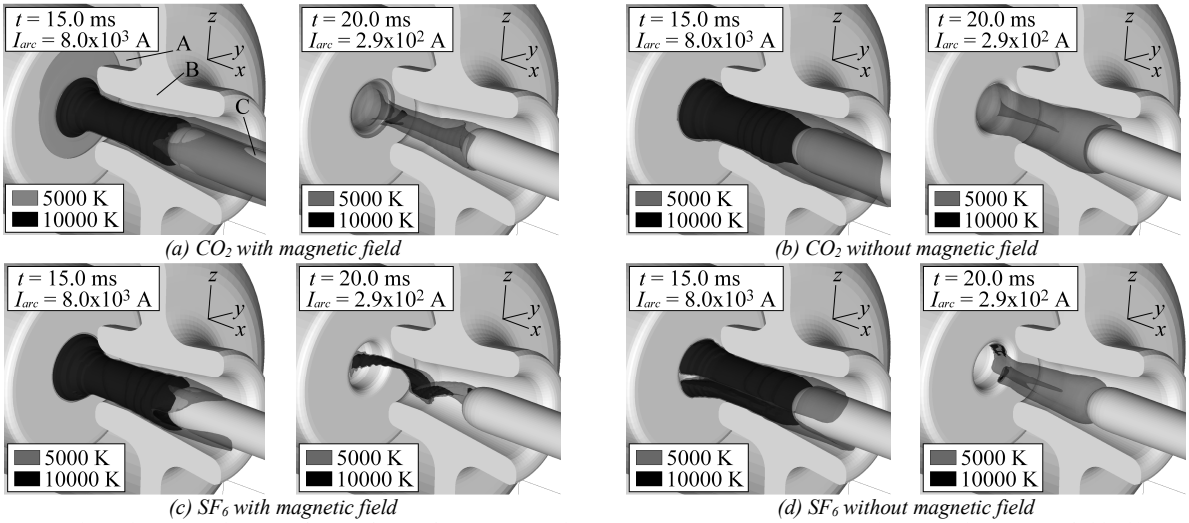

(a) CO_2 with magnetic field (b) CO_2 without magnetic field

(c) SF_6 with magnetic field (d) SF_6 without magnetic field

Fig. 4 Three-dimensional views of isosurfaces of T = 5000 and 10000 K at t = 15.0, 20.0 ms: (a) CO_2 with magnetic field, (b) CO_2 without magnetic field, (c) SF_6 with magnetic field, and (d) SF_6 without magnetic field (A is the arc-runner, B the nozzle, and C the movable arcing contact.)

cylindrical shape under the applied magnetic field just before second current zero for CO_2 gas unlike SF_6 gas where the arc column forms spiral shape.

Figure 5 shows three-dimensional distributions of Lorentz force vector and isosurface of temperature T = 5000 K with the applied magnetic field at (a) t = 15.0 ms and (b) t = 20.0 ms for CO_2 gas. Lorentz force mainly works to the circumferential direction and also the strength of the force becomes weak due to a decrease in arc current from t = 15.0 ms to 20.0 ms. Figure 6 illustrates three-dimensional distributions of velocity vector and isosurface of temperature T = 5000 K with the applied magnetic field at (a) t = 15.0 ms and (b) t = 20.0 ms for CO_2 gas. Under the magnetic field, swirl flow is induced by circumferential Lorentz force near the surface of arc-runner. Circumferential flow velocity is getting smaller from t = 15.0 ms to 20.0 ms because Lorentz force becomes weak. Figure. 7 shows the time variations of the pressure rise Δp for CO_2 gas and SF_6 gas in same puffer chamber. The sampling point of the pressure is 'point P' shown in Fig. 1 ($x = 1.0\text{x}10^{-3}$ m, $y = 4.6\text{x}10^{-2}$ m, z = 0 m). The reference value of the pressure is the initial value (p = 0.5 MPa). For both CO_2 gas and SF_6 gas, Δp is increased by applying the magnetic field. This is caused by the swirl flows as shown in Fig. 6. Δp for CO_2 gas rises up rapidly to higher level compared to that for SF_6 gas. Our numerical results, however, may estimate the pressure to be low comparing with the experiment using SF_6 gas carried out by Mori et al. [5] because the

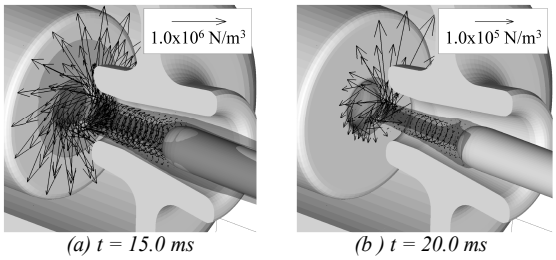

(a) t = 15.0 ms (b) t = 20.0 ms

Fig. 5 Three-dimensional distributions of vector of Lorentz force and isosurface of temperature T = 5000 K with applied magnetic field at (a) t = 15.0 ms and (b)t = 20.0 ms for CO_2.

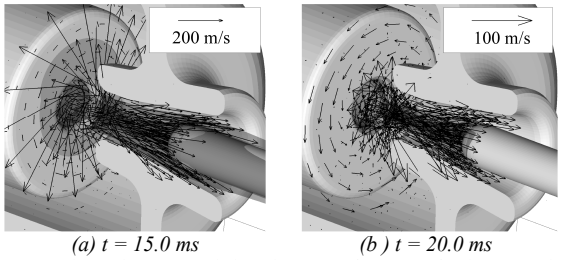

(a) t = 15.0 ms (b) t = 20.0 ms

Fig. 6 Three-dimensional distributions of vector of velocity and isosurface of temperature T = 5000 K with applied magnetic field at (a) t = 15.0 ms and (b)t = 20.0 ms for CO_2 gas.

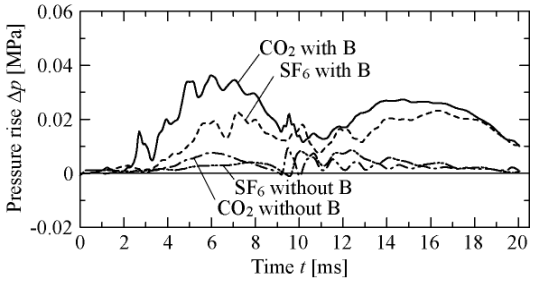

Fig. 7 Time variations of pressure rise in puffer chamber(at point P in Fig. 1)

maximum pressure rise in their experiment is about 0.2 MPa for SF_6 gas with the same magnetic field.

Here, we evaluate heat balance by the conservation equation of thermal energy Eq. (7)

derived by the governing equation of fluid Eq. (1)－(3).

$$\frac{\partial(\rho U)}{\partial t} = -\nabla\cdot(\rho U\boldsymbol{u}) + \nabla\cdot(k\nabla T) - p(\nabla\cdot\boldsymbol{u}) + (\tau:\nabla\boldsymbol{u}) + \frac{\boldsymbol{J}\cdot\boldsymbol{J}}{\sigma} - \dot{q}_{rad} \quad (7)$$

In Eq. (7), U is the internal energy per unit mass [J/kg]. In the right side of Eq. (7), from top to bottom, each term expresses convection, thermal conduction, pressure work, viscous dissipation, joule heating, and radiation heat loss. Here, the heat balance per unit length along x-axis $Q_{i,x}$ is defined as Eq. (8).

$$Q_{i,x} = \frac{1}{x'-x}\int_{V_{\sigma\geq 1}} q_i dV \quad [\mathrm{W/m}] \quad (8)$$

where q_i is the value of the i th term in the right side of Eq. (7) [W/m^3], V the volume of the region where $\sigma \geq 1\,\mathrm{S/m}$.

Figure 8 shows details of heat balances of CO_2 arc plasma along x-axis just before second current-zero point (t = 20.0 ms). As shown in Fig. 8, the convection term turns from positive to negative by applying the magnetic field between arc-runner and nozzle inlet ($x \leq 0.10\,\mathrm{m}$). This means the convection heat loss is enhanced and it promotes a drop in arc temperature. Just before second current-zero, the convection heat loss is mainly caused by the axial flow which is produced by the pressure rise in the puffer chamber rather than the other components.

Figure 9 shows relation between the arc conductance and the arc current. For both CO_2 and SF_6 gas, arc conductance is decreased by applying the magnetic field. In addition, the decreasing rate of arc conductance is increased just before current-zero by applying the magnetic field for CO_2 gas, although it is inferior to that of SF_6. This means the thermal interruption capability can be also improved by applying magnetic field for CO_2 gas.

4. CONCLUSIONS

Three-dimensional and time dependent magnetohydrodynamic numerical simulations are conducted to examine arc behavior and thermal interruption capability under the magnetic field for the gas circuit breaker using CO_2 or SF_6 gas. The main results are as follows:

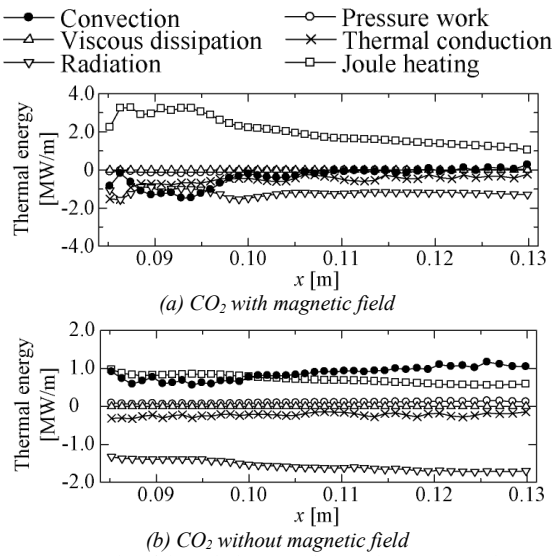

Fig. 8 Details of heat balances of arc plasma at each point along x-axis (t = 20.0 ms): (a) CO_2 with magnetic field and (b) CO_2 without magnetic field

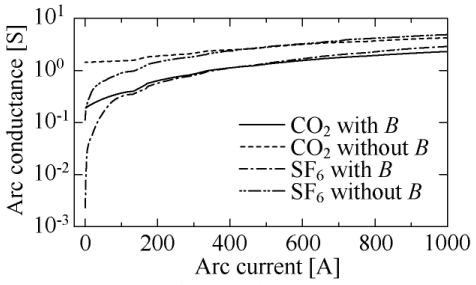

Fig. 9 Variation of arc conductance to arc current

1) For CO_2 gas, arc becomes more contracted by applying the magnetic field just before current-zero. In addition, the arc forms cylindrical shape under the magnetic field for CO_2 unlike SF_6 where the arc column forms spiral shape.

2) For both CO_2 and SF_6 gas, arc conductance just before current-zero can be effectively reduced by applying the magnetic field. This is because a rapid drop in arc temperature due to the enhancement of the convection heat loss.

REFERENCES

[1] T. Uchii, et al., IEEJ Trans. on PE, Vol. 124, No. 3, pp.469-475 2004.
[2] Patric C. Stoller, et al., IEEE Trans., Vol. 41, No. 8, pp.2359-2369, 2013.
[3] X. Y. Hu, et al., J. Comp. Phys., Vol. 219, pp. 553-578, 2006.
[4] D. Hartmann, et al., Comput. Methods Appl. Mech. Engrg., Vol. 200, pp. 1038-1052, 2011.
[5] T. Mori, et al., 7th International Workshop on High Voltage Engineering, ED-10-060, SP-10-027, HV-10-022, 2010.